Investigation on the Machinability of Metastable β Titanium Alloy M28

Yifan JIANG
Nanjing University of Aeronautics and Astronautics College of Mechanical and Electrical Engineering
Hui Tian
2. AVIC Xi'an Aircraft Industry (Group) Company LTD, Xi'an
Jia Yin
Nanjing University of Aeronautics and Astronautics College of Mechanical and Electrical Engineering
Yinfei Yang
Nanjing University of Aeronautics and Astronautics College of Mechanical and Electrical Engineering
Guolong Zhao
Nanjing University of Aeronautics and Astronautics College of Mechanical and Electrical Engineering
Liang Li (liliang@nuaa.edu.cn)
Nanjing University of Aeronautics and Astronautics College of Mechanical and Electrical Engineering

Research Article

Keywords: high-speed milling, β titanium alloy, titanium alloy machinability, carbide tools, tool wear

Posted Date: August 30th, 2021

DOI: https://doi.org/10.21203/rs.3.rs-848945/v1

Investigation on the Machinability of Metastable β Titanium Alloy M28

Yifan Jiang [1], Hui Tian [2], Jia Yin [2], Yinfei Yang [1], Guolong Zhao [1], Liang Li [1] *

1. *College of Mechanical and Electrical Engineering, Nanjing University of Aeronautics and Astronautics, Nanjing 210016, China*
2. *AVIC Xi'an Aircraft Industry (Group) Company LTD, Xi'an 710089, China*

Abstract

Oriented to the application of new generation strategic aircraft, M28 (Ti-4Al-5Mo-5V-6Cr-1Nb) is a novel metastable β titanium alloy with outstanding strength. A better understanding of its machinability is the cornerstone of the manufacture. In this work, milling experiments were made with the uncoated WC-Co carbide insert to investigate its machinability. Compared with milling Ti-6Al-4V, the cutting force is much higher and the tool life is considerably shorter in the milling of M28, especially in the high-speed cutting. Serious edge breaking is found at normal cutting speed. While a continuous band of flank wear with significant chip adhesion, which covers comb cracks in the cutting edge, is found in the high-speed cutting tool. The machinability of M28 is considerably poorer than that of Ti-6Al-4V. The hard-to-machine performance of M28 is considered to be subject to the material property of the metastable β titanium alloy as well as the competing mechanism among work hardening, strain rate hardening and the thermal softening in the cutting. According to the detection of the scanning electron microscope (SEM) and the energy dispersive spectrometer (EDS), the diffusion of C and Co generates a negative influence on the cutting edge and accelerates the tool wear.

Key words: high-speed milling; β titanium alloy; titanium alloy machinability; carbide tools; tool wear

1. Introduction

The new generation of aircraft calls for a new generation of material. Therefore, novel titanium alloys are developed to satisfy the more demanding requirement of material performance in strength-to-weight ratio, strength, fatigue strength and corrosion resistance, et al[1-3]. Increasingly more attention has been put on metastable β titanium alloys since these alloys can be hardened to extremely high strength and their complex microstructure enables the combination of both high strength and high toughness[4, 5]. β titanium alloys show good application values in the aircraft component such as landing gears, load-bearing fuselage components and high-lift devices of the large aircraft, plug-and-nozzle assemblies of the jet engine and main bolted rotor head of helicopters, et al[1-3, 6, 7].

However, the outstanding material performance poses a challenge to aircraft manufacturing. β titanium alloys have been reported to be the most difficult to machine among all titanium alloys since the 1970s[8]. β titanium alloys is hard to machine due to the elevated cutting temperature, high cutting forces, and, particularly, the rapid tool wear[9-13]. The machining efficiency of them is restricted by the tool life. For instance, to achieve an industry employed tool life (15 min), the cutting speed for machining Ti-5Al-5Mo-5V-3Cr, a typical β titanium alloy, was nearly 56% lower than that for machining Ti-6Al-4V[10]. The tool wear in cutting β titanium alloys, including Ti-5Al-5Mo-5V-3Cr, Ti-10V-2Fe-3Al and

Ti-3Al-8V-6Cr-4Mo-4Zr(βC alloy), is mainly classified as abrasion and adhesion[7, 10, 14-16]. The micro-chipping at the cutting edge was generated in the machining of aged Ti-10V-2Fe-3Al[12, 15]. Chip adhesion still occurs even various cooling and lubrication method was applied in machining β titanium alloys, including liquid nitrogen cryogenic cooling, high pressure fluid cooling, minimum quantity lubrication (MQL) [17, 18] and carbon dioxide snow jet cooling[7].

As a novel titanium alloy with an outstanding strength as high as 1350MPa[2], M28 (Ti-4Al-5Mo-5V-6Cr-1Nb) is applied in the load-bearing fuselage component of the new generation strategic aircraft. Besides the common features of titanium alloys, such as poor thermal conductivity, high chemical reactivity, and low modulus of elasticity[12, 19], the machining of M28 is subject to the specific property of metastable β titanium alloys as well. The machinability evaluation is the cornerstone of machining efficiency improvement. The knowledge about the cutting tool wear behavior in machining M28 will also contribute to the understanding of the ultra-high strength titanium alloy cutting process.

In this study, milling experiments of M28 were conducted with the uncoated WC-Co carbide insert to investigate its machinability. To research the wear mechanism of high-speed cutting of M28, microscopic observations of the worn edge were made. In addition, the worn insert was sectioned to analyze the element distribution across the tool-chip interface in the wear area.

2. Experiment procedures

2.1 Workpiece materials

M28 (Ti-4Al-5Mo-5V-6Cr-1Nb) is a novel metastable β titanium alloy[2]. The chemical composition of the as-received M28 material is listed in **Table 1**. β stabilize elements such as V, Mo and Nb play the role of strengthening elements due to their high solid solubility in β phase[20].

Table 1 Chemical composition of the workpiece (wt.%)

Al	Mo	V	Cr	Nb	Ti
3.73	4.98	4.09	5.82	1.08	Balance

Molybdenum equivalent (Mo_{Equ}) is utilized for ranking the β phase stability of various compositions, indicating the capacity to obtain an ultimate strength and hardness in the aged condition [10, 21]. Its calculation equation is shown in Eq.(1) [22]. In general, a Mo_{Equ} of 10 is required to stabilize the β phase upon quenching to room temperature[23]. The nominal composition of the M28 alloy, Ti-4Al-5Mo-5V-6Cr-1Nb, has a Mo_{Equ} of 14.23%, which is much larger than that of Ti-6Al-4V (a typical $\alpha+\beta$ titanium alloy) and Ti-10V-2Fe-3Al (a typical β titanium alloy), as shown in **Fig. 1**. Therefore, M28 can retain the body-centered cubic (BCC) structure at room temperature.

$$\mathrm{Mo}_{Equ} = \mathrm{Mo} + 0.67\mathrm{V} + 0.44\mathrm{W} + 0.28\mathrm{Nb} + 0.22\mathrm{Ta} + 2.9\mathrm{Fe} + 1.6\mathrm{Cr} - \mathrm{Al} \quad (1)$$

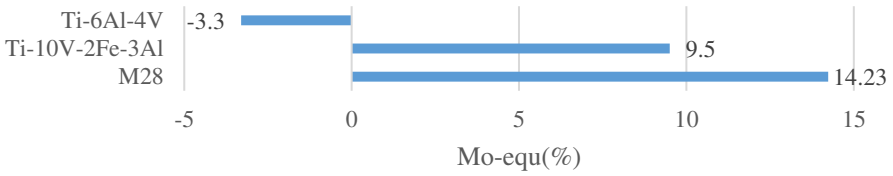

Fig. 1 Mo_{Equ} of three kinds of titanium alloys[2]

Mechanical properties of metastable β titanium alloys can be tailored by controlling the microstructure via heat treatments. Through aging treatment, fine secondary α phase (bright speckles in the β phase) uniformly precipitated in coarse equiaxed β grains, as shown in **Fig. 2**. The comparison among the strength of M28, Ti-6Al-4V and Ti-10V-2Fe-3Al is shown in **Fig. 3**. The strength of aged M28 is as high as 1350 MPa, much higher than that of Ti-6Al-4V and Ti-10V-2Fe-3Al.

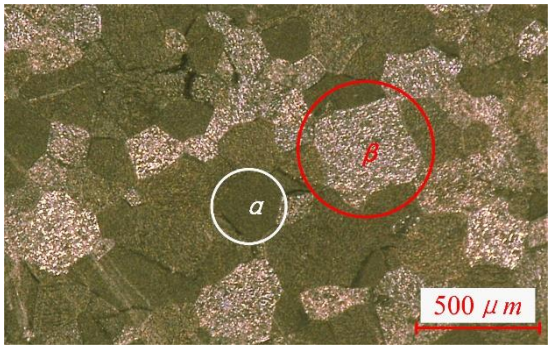

Fig. 2 Metallographic image of aged M28

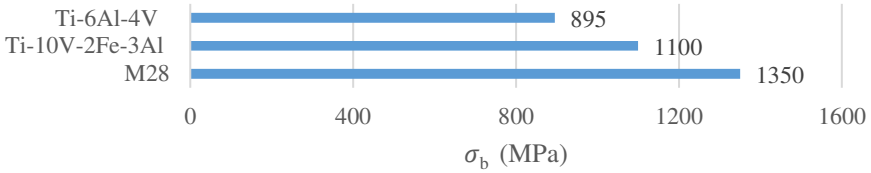

Fig. 3 Strength of three kinds of titanium alloys [1, 2]

2.2 Cutting tool, machine tool and cutting parameters

On-shelf uncoated cutting inserts in ISO grade K40 were utilized for the experiment. The composition of this carbide is mainly WC and Co (6%, wt). The geometry of the insert is listed in **Table 2**. The tool diameter is 25mm. In the experiment, only one insert was equipped on the tool each time in the cutting experiment.

Table 2 Geometry parameters of the K40 insert

Rake angle γ	Clearance angle α	Cutting edge angle K_r	Helix angle β
25°	15°	90°	0°

The experiments were carried out on a high-speed machining center Mikron UCP 710, supplying a maximum power of 16 kW and a maximum spindle speed of 18,000 rpm. The cutting force of milling M28 was tested at varying cutting speeds v_c and feed per tooth f_z respectively, with the constant cutting depth a_p and cutting width a_e. The cutting parameters of the tests are listed in **Table 3** and **Table 4**.

Table 3 Cutting parameters of the cutting force test at varying cutting speeds

Material	v_c (m/min)	f_z (mm/z)	a_p (mm)	a_e (mm)
M28	45	0.1	5	1
	60			
	100			
	200			
	300			

Table 4 Cutting parameters of the cutting force test at varying feeds per tooth

Material	v_c (m/min)	f_z (mm/z)	a_p (mm)	a_e (mm)
M28	200	0.06	5	1
		0.08		
		0.1		
		0.12		
		0.15		

Cutting speed is considered as the priority factor for tool wear[24]. In this research, contrast tests of milling M28 and Ti-6Al-4V about the influence of the cutting speed on the tool wear were carried out. The cutting parameters of the contrast tool wear test is listed in Table 5. A 0.3 mm width of the flank wear VB was set as the tool wear criteria. The cutting length L_c of each insert was documented as the flank wear reaches the wear criteria.

Table 5 Cutting parameters of the tool wear contrast test

Material	v_c (m/min)	f_z (mm/z)	a_p (mm)	a_e (mm)
M28 & Ti-6Al-4V	45	0.1	5	1
	100			
	200			
	300			

2.3 Measurement and detection

Cutting forces in an orthogonal coordinate (Fx, Fy, Fz) were measured by a piezoelectric dynamometer (Kistler 9265B) and the charge amplifier (Kistler 5019A) at the sampling rate of 10kHz. **Fig. 4** illustrates the experiment set up, the cutting force in the X-direction (Fx) was parallel to the feed speed vf, the cutting force in Y-direction (Fy) was parallel to the cutting width a_e and the cutting force in the Z-direction (Fz) is in the spindle direction. The cutting force signal was recorded through an A/D converter on a standard desktop PC with the data acquisition and processing software

Dynoware. In this paper, the mean value of the maximum force data is counted as the cutting force value.

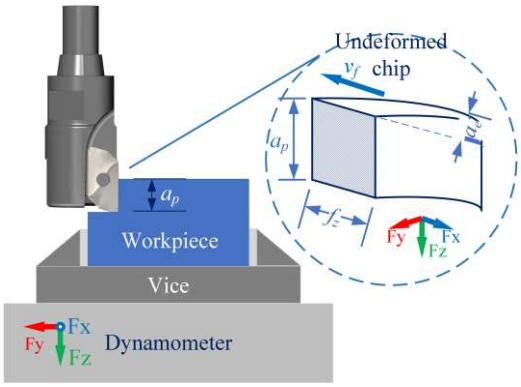

Fig. 4 Experimental setup for cutting force measurement

A CCD microscope (CXSP-2KCH) was utilized to observe and measure the flank wear in the experiment. To uncover the worn edge under the titanium material adhesion, the adhesion material was pickled by the hydrofluoric etchant. The microscopic observation and element detection of the worn edge was carried out by a Hitachi TM 3000 scanning electron microscope (SEM) with an energy-dispersive spectrometer (EDS) system (Oxford Instruments). To further investigate the tool wear, a worn insert was sectioned perpendicular to the cutting edge by electrical discharge machining (EDM) to reveal the inner part of the worn edge, as shown in **Fig. 5**. The sectioned insert was encapsulated in the conductive resin and polished with diamond spray.

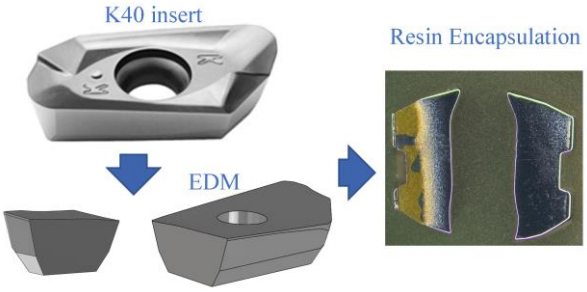

Fig. 5 Cross-sectioned insert sample

3. Results and discussion

3.1 Cutting forces

Cutting forces directly reflect the cutting process, hence the knowledge of the development low of it is beneficial to process design. **Fig. 6** shows the influence of the cutting speed on the cutting force. Fy (in the cutting width direction) is the dominant proportion of the 3-dimensional cutting forces, following Fx (in the feed direction). Fy rises considerably with the increasingly growing cutting speed, especially in the high-speed cutting (v_c ≥100 m/min), while the increase of Fx and Fz is not so distinguished. **Fig.**

7 shows the influence of the feed per tooth on the cutting force at v_c= 200 m/min. With the increase of the feed per tooth, Fy rises in an approximate linear pace. Similarly, the increase of Fx and Fz is less significant than that of Fy. Fy mainly originates from the interaction between the side cutting edge and the finished workpiece surface. Due to the low elasticity modulus of titanium alloys (the elasticity modulus of M28 is 103 GPa while that of Ti-6Al-4V is 114 GPa[25]), the finished surface will rebound on the flank face of the side edge. With the higher cutting speed, Fy will increase as the rebound goes stronger.

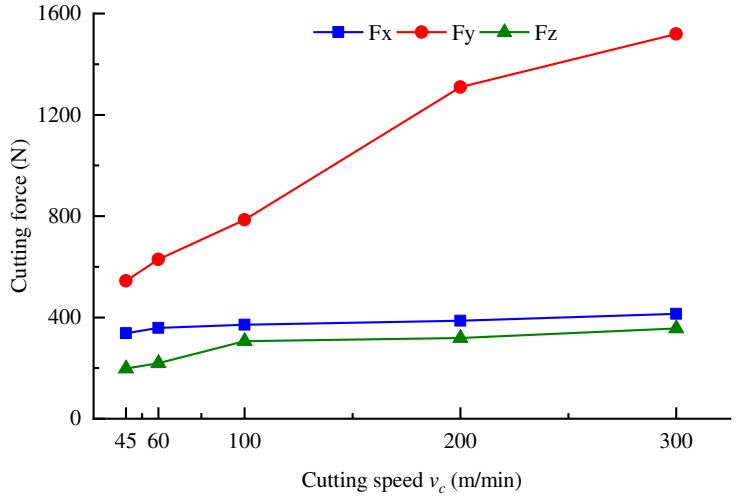

Fig. 6 Cutting forces VS. cutting speed (f_z=0.1 mm/z, a_p=5 mm, a_e=1 mm)

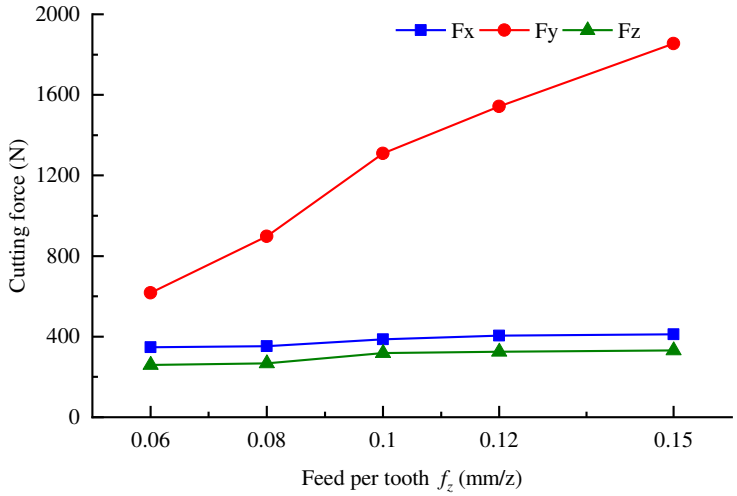

Fig. 7 Cutting forces VS. feed per teeth (v_c=200 m/min, a_p=5 mm, a_e=1 mm)

Cutting forces originates from the interaction of the cutting tool and workpiece material. Under the same conditions of the tool and cutting parameters, the comparison of the cutting force reveals the machining property of M28. As **Fig. 2** shows, the microstructure of M28 is mainly composed of coarse equiaxed β grains filled by fine secondary α phases. This secondary phase precipitation is a consequence of thermodynamic instability associated with metastable β titanium alloys[26]. Fine

secondary α precipitations obtained after aging treatments could result in high strength due to the strong resistance of α/β interface to dislocation movement[20]. Such age-hardening effect [2, 5] imparts M28 the ultra-strength. A mixture of coarse primary α phase and fine secondary α phase can cause inhomogeneous slip distribution[4], thus increases the toughness of M28. Furthermore, titanium alloy is subject to considerable work hardening and strain rate strengthening in the rapid plastic deformation process like high-speed cutting[27, 28]. These factors contribute to the high cutting force in the cutting of M28.

3.2 Tool wear

Fig. 8 presents cutting forces of M28 and Ti-6Al-4V in the tool wear test. Fx of M28 is almost 85% of that of Ti-6Al-4V from the cutting speed of v_c =45 m/min to v_c =300 m/min. Fy of M28 at the cutting speed of v_c=45 m/min is nearly 115% of that of Ti-6Al-4V. However, in the high-speed cutting, Fy of M28 shows a percentage rise which will increases as high as 132% of that of Ti-6Al-4V at the cutting speed of v_c =300 m/min. While Fz of M28 at the cutting speed of v_c=45 m/min is nearly 136% of that of Ti-6Al-4V. With the cutting speed increasing, Fz of M28 slightly rise to 154%,143% and 152% of that of Ti-6Al-4V at the cutting speed of v_c =100 m/min, v_c =200 m/min and v_c =300 m/min, respectively.

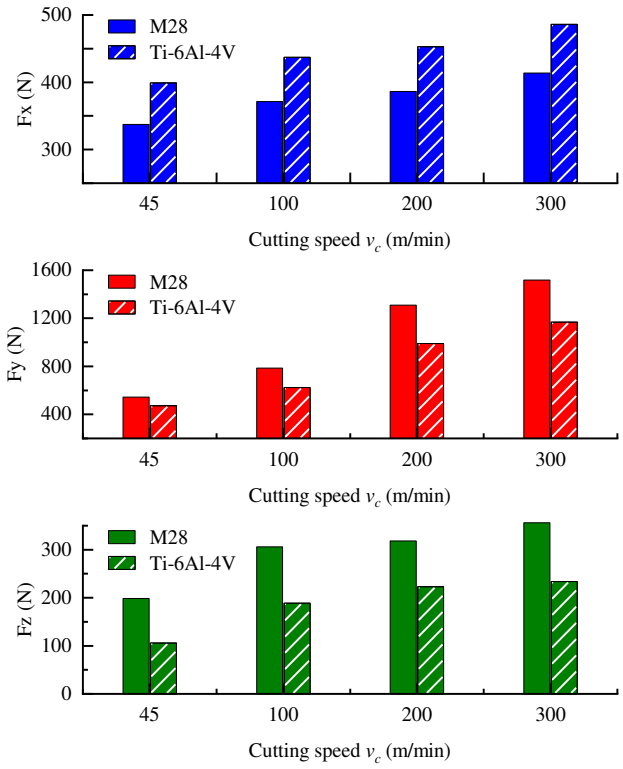

Fig. 8 Cutting forces of M28 and TC4 in varying cutting speeds (f_z=0.1 mm/z, a_p=5 mm, a_e=1 mm)

The tool life of milling M28 and Ti-6Al-4V in the same cutting speed were presented in **Fig. 9**. The cutting length at a lower cutting speed is longer than that at a higher cutting speed in both the machining of M28 and Ti-6Al-4V. In the machining of M28, the reduction in the cutting speed brings a significant effect on the tool life as compared with machining Ti-6Al-4V. For M28 machining, the cutting length at

the cutting speed of v_c=45 m/min is nearly 495% of that at the cutting speed of v_c=300 m/min. The tool life of M28 is considerably poorer than that of Ti-6Al-4V in the same condition of cutting parameters and tool. The cutting length of milling M28 is nearly 0.88% of that of Ti-6Al-4V at the cutting speed of v_c=45 m/min. In the high-speed cutting, the percentage comes to be 4.02%, 6.21% and 13.82% of that of Ti-6Al-4V at the cutting speed of v_c=100 m/min, 200 m/min and 300 m/min respectively. The comparison in tool life, as well as the higher cutting force, presents the poor machinability of M28 directly.

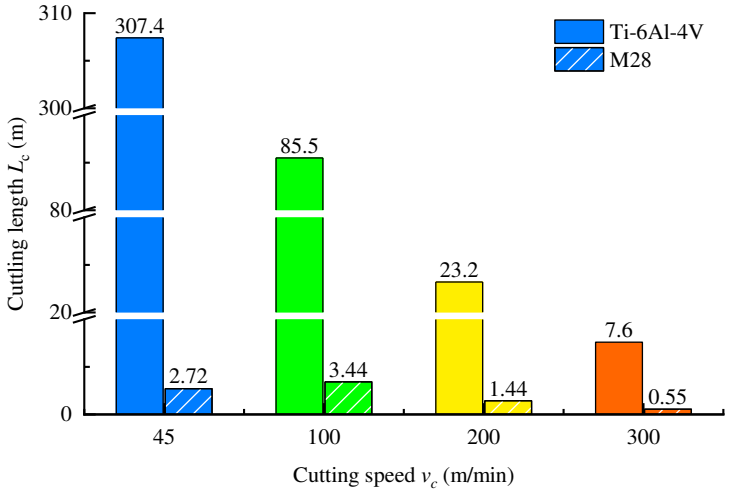

Fig. 9 Cutting length of M28 and Ti-6Al-4V in varying cutting speeds (f_z=0.1 mm/z, a_p=5 mm, a_e=1 mm)

Fig. 10 presents the development of tool flank wear of cutting M28 at varying cutting speeds. The increasement of the flank wear is rapid in the high-speed cutting, especially at the cutting speed of v_c =300 m/min and v_c =200 m/min. At the cutting speed of v_c =45 m/min, the development of VB is slower than that at the cutting speed of v_c =100 m/min before a rapid rise. This is due to the cutting-edge chipping. As the worn edges at varying cutting speeds shows in **Fig. 11**, there is a distinguishable difference between the wear mode in the normal speed cutting and that of the high-speed cutting. At the cutting speed of v_c = 45 m/min, large scale edge chipping occurs with some adhesion material remaining in the broken flank face, as shown in **Fig. 11**a). While continuous bands of flank wear are formed with significant chip adhesion on it at the cutting speed of v_c = 100 m/min, v_c = 200 m/min and v_c = 300 m/min, as shown in **Fig. 11**b), c) and d) respectively. These chip adhesion covers almost all the engaged edge

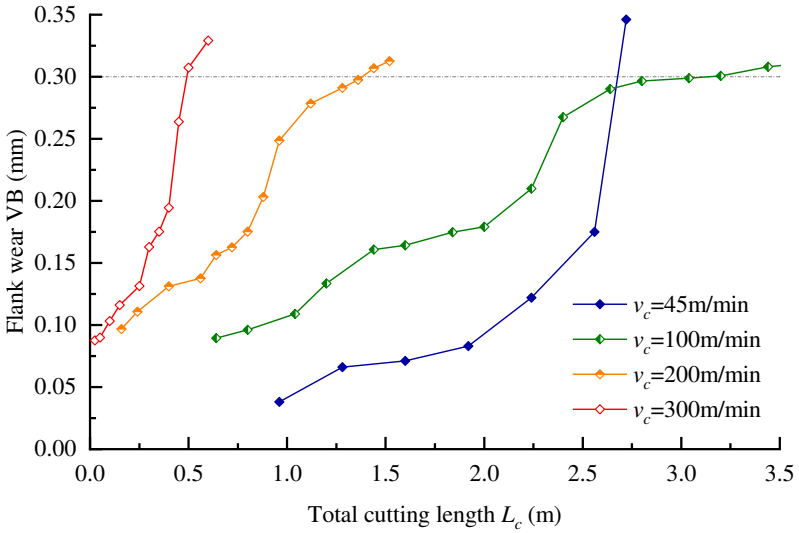

Fig. 10 Flank wear development in varying cutting speeds (f_z=0.1 mm/z, a_p=5 mm, a_e=1 mm)

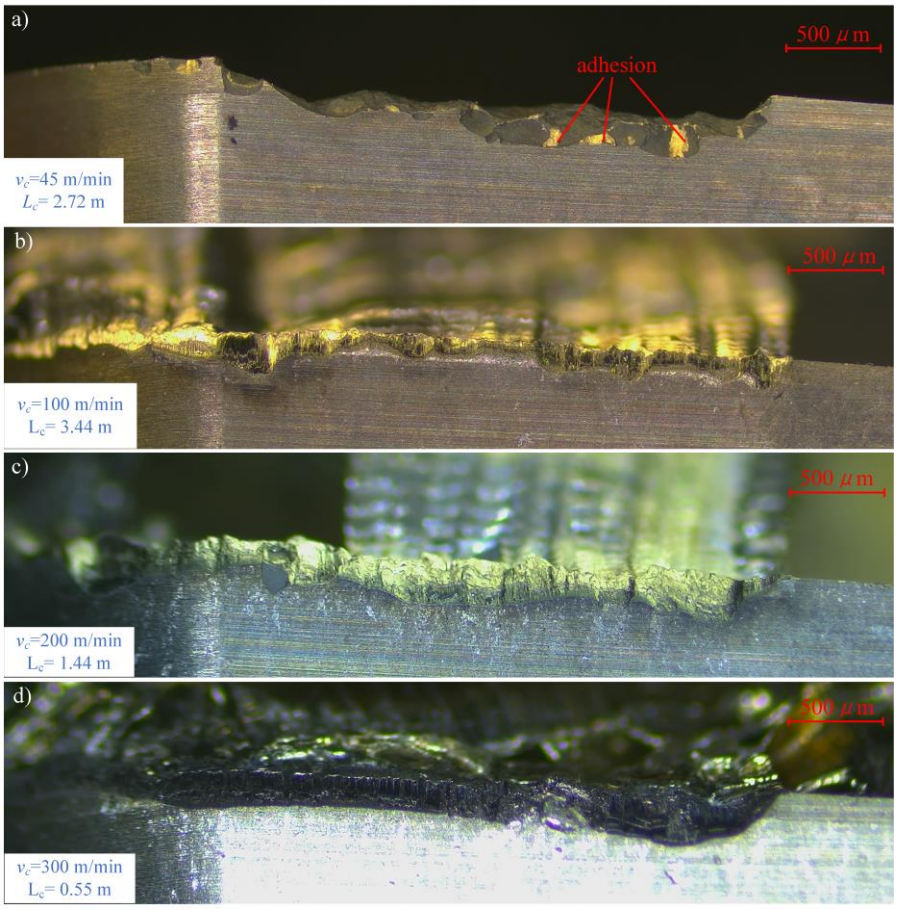

Fig. 11 Tool wear at varying cutting speeds a) v_c = 45 m/min, b) v_c = 100 m/min, c) v_c = 200 m/min and d) v_c = 300 m/min

The SEM image of the adhesion on the worn tool edge at the cutting speed of v_c = 45 m/min is shown in **Fig. 12**. Cutting edge chipping can be found in the flank face as shown in **Fig. 12** a). In the broken area there exists some amount of adhesion material. The cascading adhesion material, as shown in **Fig. 12**b), indicating it is a part of the chip flow. The cutting edge lost its sharpness due to the material chipping,

however the newly formed irregular edge in the broken area takes the place of it and proceeds with cutting. **Fig. 13** presents the EDS image of a chip collected in the experiment (v_c = 45 m/min), there is a small piece of carbide embedding in the chip.

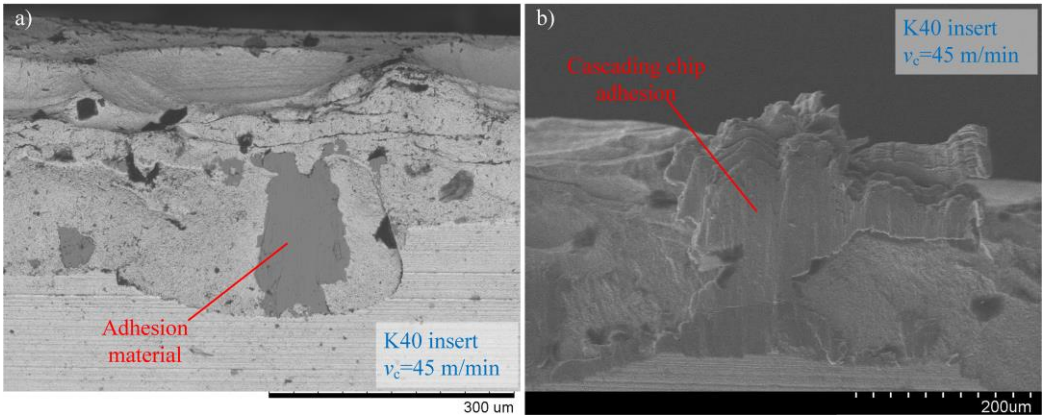

Fig. 12 Worn edge at v_c=45 m/min, a) Adhesion in the broken area and b) Cascading chip adhesion

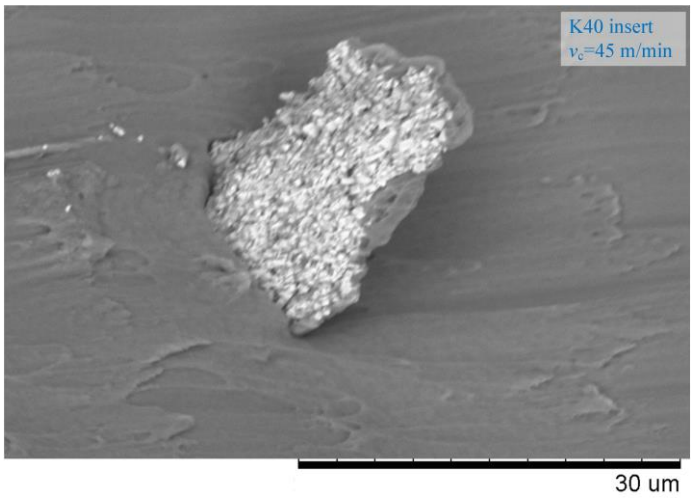

Fig. 13 Carbide piece in the chip

In the high-speed cutting experiment, the cascading chip flow adhered along the whole engaged cutting edge, as shown in **Fig. 15**. The spectrum of chemical elements at point A and point B of the adhesion chip material are presented in **Fig. 16** a) and b) respectively. W, C and Co are found at the chip adhesion indicating the diffusion of carbide material.

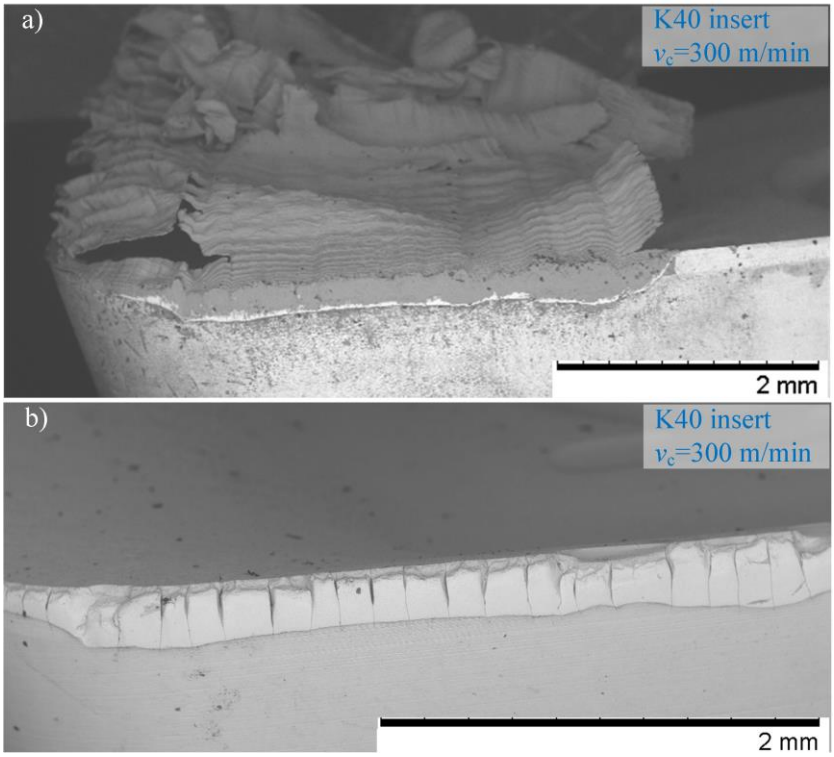

Fig. 14 Worn edge in high-speed cutting, a) cascading chip adhesion and b) comb cracks

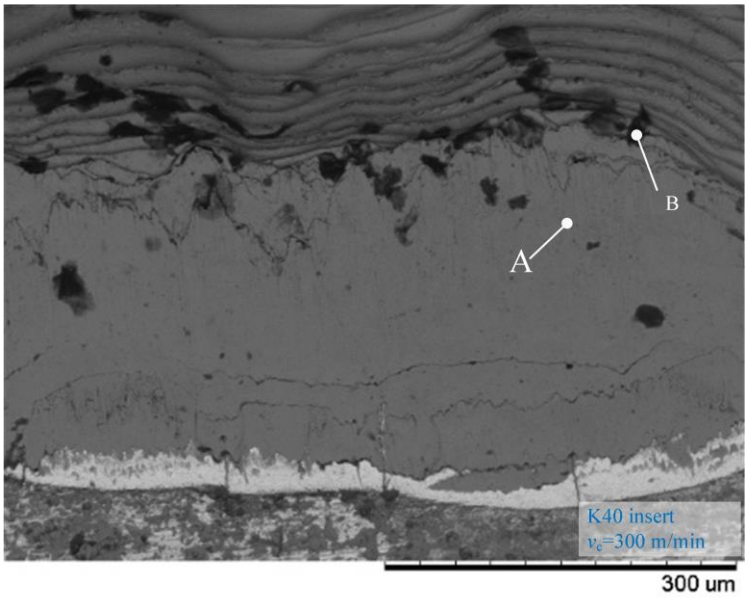

Fig. 15 Chip adhesion on the worn edge

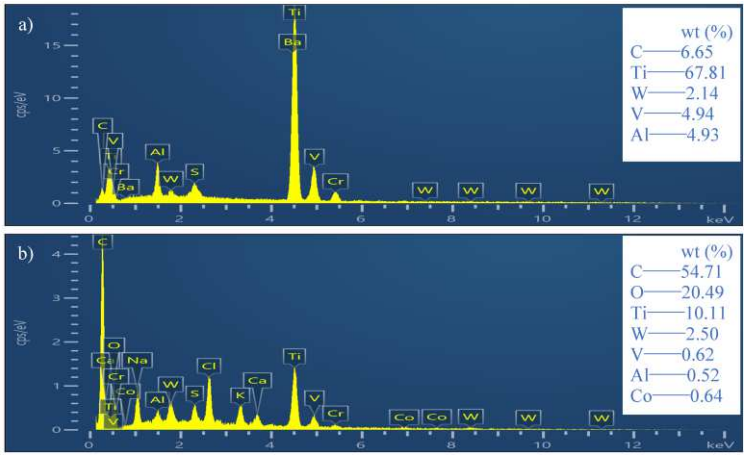

Fig. 16 EDS spectrum a) point A and b) point B

Comb cracks along the whole engaged cutting edge reveal after the chip adhesion is etched, as shown in **Fig. 14** b). In the case of high-speed milling, the carbide material is subject to strong alternating thermal stress, which leads to the comb crack in the cutting edge[24].On the top of the worn edge, there are semi-carters like concave corners, as shown in Fig. 17.

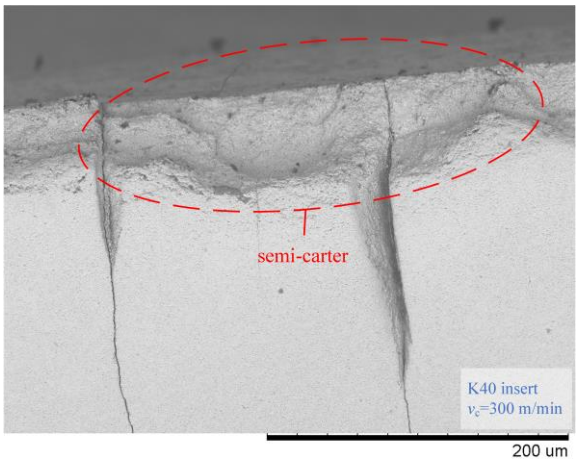

Fig. 17 Semi-carter in the worn edge

Some scattered WC particles are found on the surface of the adhesion chip, as Fig. 18 shows. The chemical elements of a single particle (point C) are presented in Fig. 19. The major element of it is W and C, while some other elements from M28, including Ti, Al, and V are also found. Co acts as the binder phase to hold the WC particles in the carbide[29]. The scattered WC particles as well as the Co detected in chip adhesion, as shown in **Fig. 15**, indicate the diffusion of Co. As the Co diffused to the chip adhesion, the holding to the WC particles is weakened[15, 30-32], so the loosened WC particles can be dropped out easily by the chip flow. The semi-carter was possibly formed by the diffusion of carbide and the erosion of chip flow.

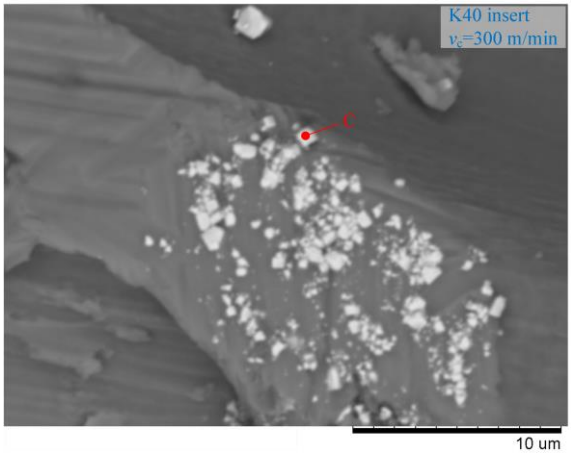

Fig. 18 WC particles in the chip

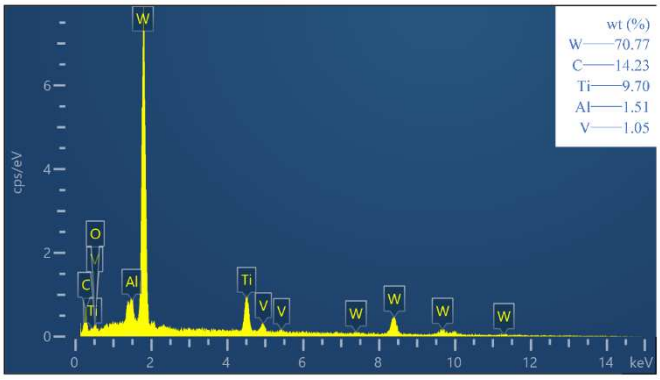

Fig. 19 EDS spectrum of point C

The EDS image of the sectioned-profile K40 insert is shown in **Fig. 20**. The original sharp edge has been worn to be irregularly round. At the tip of it adheres a little chip material. The irregularly rounded edge is approximately composed of circular arcs with radios 215.41μm and 250.43μm, respectively.

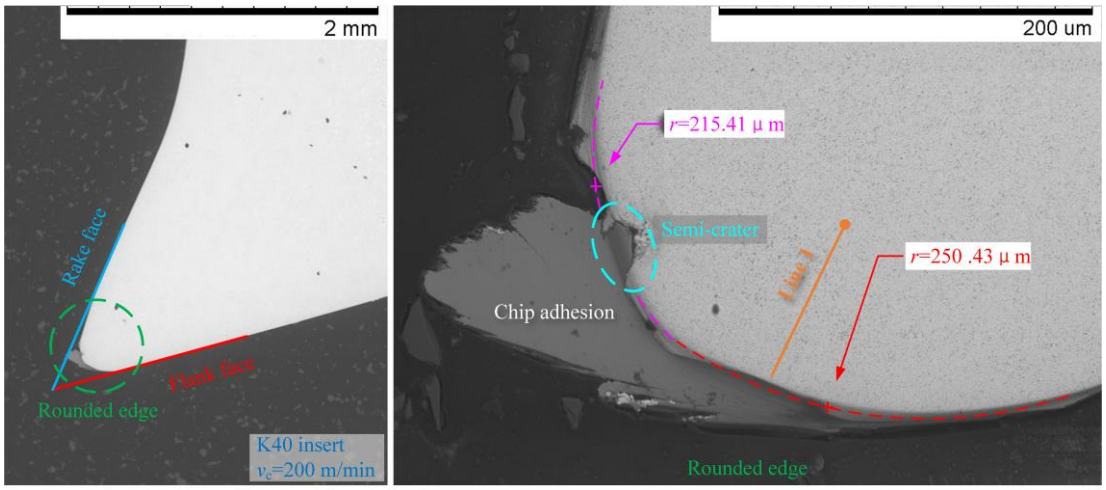

Fig. 20 Rounded edge with chip adhesion

The chemical element distribution in the flank face surface to the inner matrix was detected by EDS

line-scanning, as shown in **Fig. 21**. Gradient distributions of W and C are found through the superficial layer of the tool-workpiece interface to the inner matrix. An isolated peak in the Ti spectrum curve is located at approximately 30~40 μm from the flank face with a spectrum curve peak of C. As **Fig. 21** shows, the distribution of chemical elements at the flank face can be divided as the rich carbon layer (RC layer), the diffusion layer and the carbide matrix (WC+Co), from the superficial of the flank face to the inner matrix sequentially. The RC layer ranges about 30 μm from the flank face. The diffusion layer is located beneath the RC layer, covering a width of 20~30 μm with element concentration gradient gap. The isolated titanium peak lies in this layer.

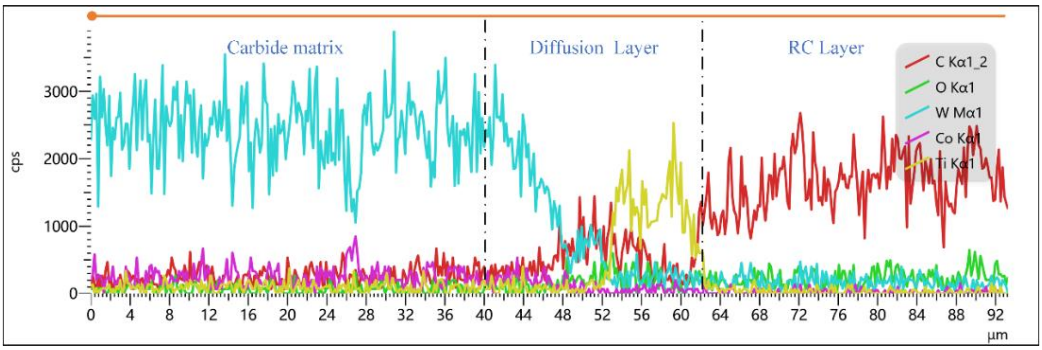

Fig. 21 Elements distribution in Line 1

The symmetrical section profile of the insert is shown in **Fig. 22**. On the rounded edge, there is a crack through the edge tip. In the symmetrical section profile of the insert, a similar isolated CPS peak of Ti is also found in the scanning spectrum of Line 2, as shown in Fig. 23. The isolated CPS peak of Ti indicates the titanium material filling in it. Since K40 carbide contains only WC and Co, the titanium material can only originate from the chip flow. Comb cracks act as access to the inner side of the insert.

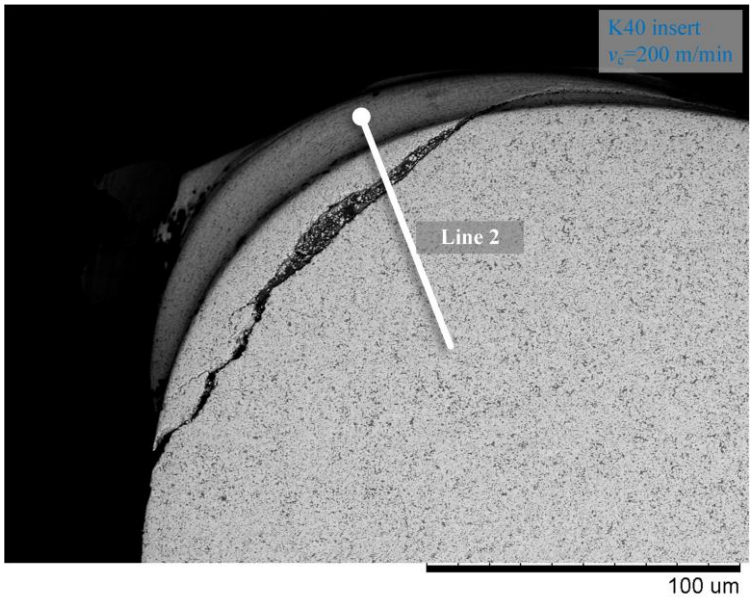

Fig. 22 Symmetrical section-profile of the insert

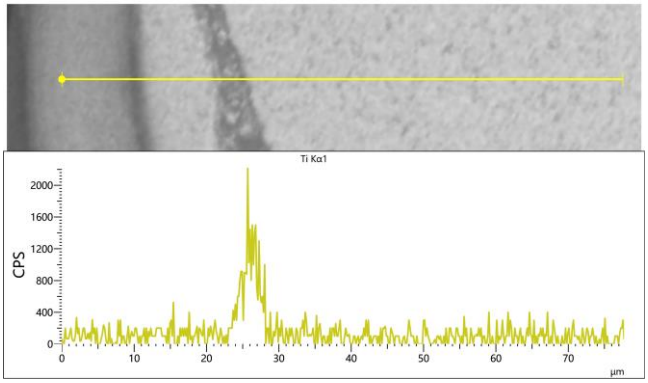

Fig. 23 Ti spectrum in Line 2

Fig. 20 The semi-crater is filled with the material from chip adhesion, as the SEM image shows in **Fig. 24**. Crater wear usually occurs in the rake face of the carbide tool for turning with a quite larger size than the semi-crater found in the experiment [32-34]. An EDS line scanning was made in the semi-crater profile to reveal the trace of chemical elements as shown in **Fig. 25**. In the carbide side of the tool-chip interface, the content of W and Co is relatively low. This may be caused by the diffusion of Co and loss of W in the superficies of the tool. The C spectrum peak indicates a carbon enrichment. While a slight trace of Ti is shown on the carbide side. There may be a little amount of Ti diffusion into the carbide. In the high-speed cutting, the heat softened chip adheres on the edge tip then the diffusion launches. Thus the semi-crater is formed since the carbide is weakened by the diffusion and the loosened carbide matrix is taken away by the chip flow.

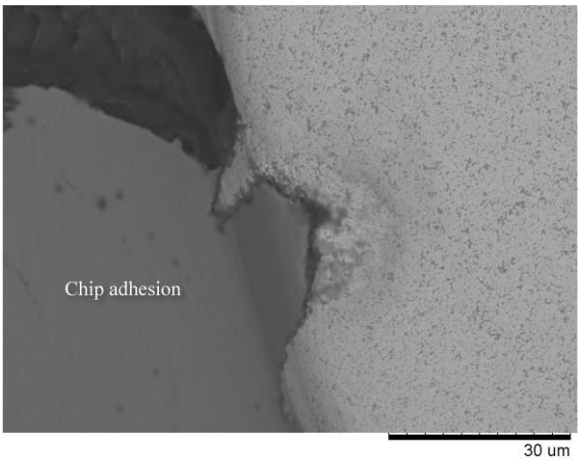

Fig. 24 Semi-crater

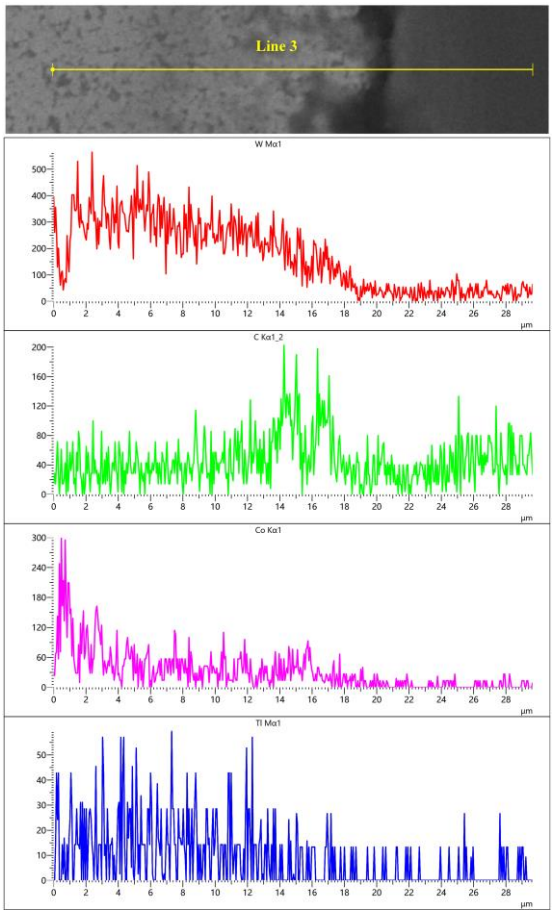

Fig. 25 Element spectrums in Line 3

3.3 Tool wear mechanism

Serious edge breaking occurs in the cutting edge with normal cutting speed, while in the high-speed cutting there forms a continuous band of flank wear, as shown in **Fig. 11**. The difference in tool wear mode shows a correlation in v_c. From the view of material properties, for the metastable β titanium alloy, high proportions of secondary α particles precipitated in the β phase works as the strengthening phase after aging treatment, accelerating the abrasive wear[11, 12]. The concentration of stress in local tiny defects is caused by the abrasive wear consequently. As a result, the edge breaking will be aggravated. The plastic deformation process of titanium alloy is subject to the competing mechanism among work hardening, strain rate hardening and thermal softening[27]. As work hardening and strain rate hardening of M28 is launched more intensely with the higher cutting speed, huge amount of heat converted from the metal plastic work will promote the softening of M28 material in the shear zone. As the thermal softening starts, the strengthening phase abrasive wear will be suppressed and the tool wear mode will also change. Considering the increasing cutting forces with the growing cutting speed, the thermal softening in the competing mechanism is not the dominant one, but still plays a certain role in the wear mode.

The mode of cutting-edge wear in the high-speed cutting of M28, as illustrated in Fig. 26, is an interaction pross of mechanical load and chemical diffusion in the cutting.

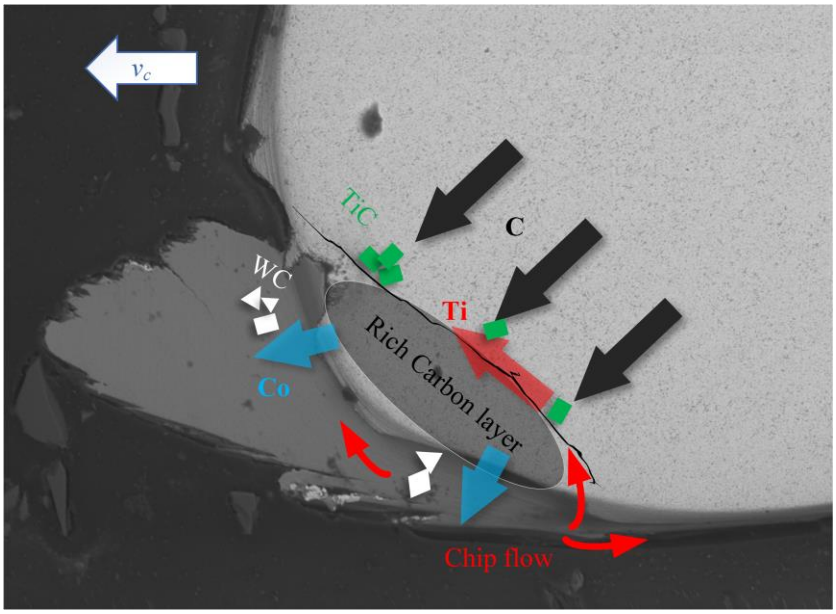

Fig. 26 Tool wear schematic in high-speed cutting

As a tiny region sensitive to the concentration of stress, the tool edge tip will be easily rounded by the wear in cutting, as **Fig. 20** and **Fig. 22**shows. The chip flow behavior in the area of the cutting edge is significantly influenced by edge shape and size [35, 36]. The rounded edge offers chip flow more contact area. Due to the high temperature and huge pressure in the cutting zone, the chip flow adheres on the flank face as **Fig. 14** shows.

The chip adhesion with the high temperature and pressure in the cutting enables the tool element diffusion. The kinetically driven decarburization of carbide will occur according to the following reactions [37]:

$$2WC \rightarrow W_2C + C \tag{2}$$

$$W_2C \rightarrow 2W + C \tag{3}$$

C will migrate into the superficial layer of the flank face due to the strong chemical reactivity of Ti[31][31]. However, the variation in the carbon content of tungsten carbide can alter the phase composition and affects the carbide properties[38]. With the enrichment of C in the superficial layer, additional graphite and the η-phase will emerge and lead to a substantial drop in hardness and wear resistance of the carbide due to the negligible strength of graphite [38-41]. The crack in the edge tip, as shown in **Fig. 22**, indicates the strength degradation of carbide in the superficial RC layer. In addition, the diffusion of Co will loosen WC particles in the carbide matrix. With the continuous chip flow rushing and dropping, semi-carters are formed at the tip of the cutting edge as **Fig. 17** shows.

The chip flow is squeezed into the inner location of the cutting edge through the comb cracks in the flank face under the high temperature and pressure in the cutting zone. Hence the trace of Ti appears in the inner side of the flank face, as the EDS spectrum shows in **Fig. 21**. The diffused C from the carbide can easily combine with the Ti as the reaction shown in Eq.(4) and Eq.(5) [15]. In the diffusion layer, as

shown in **Fig. 21**, the overlapped CPS peaks of Ti and C spectra indicate the compound of Ti and C.

$$WC + Ti = W + TiC \tag{4}$$

$$Ti + C = TiC \tag{5}$$

TiC works as a boundary inhibiting further chemical element diffusion[42-44]. However, considering the continuous chip flow, the possibility that TiC might be rushed by the chip flow in the dynamic cutting process should not be discounted.

Under the combined effect of these factors, the cutting edge will no longer maintain its original material properties and sharp geometry. With the process going on, the tool wear goes increasingly serious.

4. Conclusions

Machinability of the novel metastable β titanium alloy M28 (Ti-4Al-5Mo-5V-6Cr-1Nb) is evaluated in the experiment from the view of cutting force and tool wear. Conclusions can be drawn as follows：

1) The cutting force of milling M28 grows significantly with the increasing cutting speed, especially in the high-speed cutting. In the same cutting condition, the cutting force in the feed direction of M28 is nearly 85% of that of Ti-6Al-4V, for the cutting force in the cutting width direction the percentage ranges from 115% to 132%, and for the cutting force in the spindle direction the percentage ranges from 36% to 154%.

2) The tool life of milling M28 is considerably shorter than that of Ti-6Al-4V, no matter at the normal speed cutting or the high-speed cutting. At the cutting speed of v_c=45 m/min, the total cutting length of milling M28 is almost 0.88% of that of Ti-6Al-4V. While the percentage comes to nearly 14% at the cutting speed of v_c = 300 m/min. For milling M28, the wear mode of the carbide tool is affected by the cutting speed. At the normal cutting speed (v_c=45 m/min), serious edge chipping occurs in the flank face. When it comes to high-speed cutting ($v_c \geq$100 m/min), a continuous band of flank wear will be formed with significant chip adhesion covering comb cracks in the whole engaged cutting edge. Semi-carters are found at the tip of the edge as a result of diffusion wear.

3) The higher cutting force and considerably shorter tool life with the comparison of milling Ti-6Al-4V in the same cutting parameters and the cutting tool shows the poor machinability of M28. The material property of metallographic structure and aging -hardening effect of M28 contributes to the high cutting force and serious wear. In addition, the competing mechanism among work hardening, strain rate hardening and the thermal softening in titanium alloy cutting also affects the cutting force and tool wear mode. The thermal softening in the cutting is not the dominant one but still plays a certain role in the tool wear.

4) In the high-speed cutting of M28, the diffusion of C and Co from the carbide to the tool-chip interface is found. A rich carbon layer is formed at the superficial layer of the tool flank face, leading to the degradation in hardness and wear resistance of the carbide. A crack through the edge tip is found in the sectioned profile. As the Co diffuses, scattered WC particles are dropped by the chip flow due to the

binder phase loss.

Acknowledgments

This work is sponsored by the National Natural Science Foundation of China (No. 52075251).

References

[1] ZHU ZS. (2013) Research and development of new-brand titanium alloys of high performance for aeronautical applications. Aviation industry Press, Beijing [in Chinese]

[2] CHEN W, LIU YX, LI ZQ. Research status and development trend of high-strength β titanium alloys. Journal of Aeronautical Materials 2020; 40(03):63-76 [in Chinese]

[3] Cotton JD, Briggs RD, Boyer RR, et al. (2015) State of the Art in Beta Titanium Alloys for Airframe Applications. JOM 67(6):1281-303. https://doi.org/10.1007/s11837-015-1442-4

[4] Leyens C, Peters M.(2003) Titanium and Titanium Alloys. Wiley-VCH Weinheim. https://doi.org/10.1002/3527602119.ch2

[5] Yumak N, Aslantaş K. (2020) A review on heat treatment efficiency in metastable β titanium alloys: the role of treatment process and parameters. Journal of Materials Research and Technology 9(6):15360-80. https://doi.org/10.1016/j.jmrt.2020.10.088

[6] Singh P, Pungotra H, Kalsi NS.(2017) On the characteristics of titanium alloys for the aircraft applications. Materials Today: Proceedings 4(8):8971-82. https://doi.org/10.1016/j.matpr.2017.07.249

[7] Machai C, Biermann D.(2011) Machining of β-titanium-alloy Ti–10V–2Fe–3Al under cryogenic conditions: Cooling with carbon dioxide snow. Journal of Materials Processing Technology 211(6):1175-83. https://doi.org/10.1016/j.jmatprotec.2011.01.022

[8] Zlatin N, Field M. (1973) Procedures and Precautions in Machining Titanium Alloys. In: Jaffee RI, Burte HM, editors. Titanium Science and Technology. Springer US, Boston, 489-504. https://doi.org/10.1007/978-1-4757-1346-6_37

[9] Machai C, Biermann D.(2011) Machining of a hollow shaft made of β-titanium Ti-10V-2Fe-3Al. Proceedings - 2011 IEEE International Symposium on Assembly and Manufacturing, ISAM 2011:1-6. doi: 10.1109/ISAM.2011.5942364

[10] Arrazola PJ, Garay A, Iriarte LM, Armendia M, Marya S, Le Maître F.(2009) Machinability of titanium alloys (Ti6Al4V and Ti555.3). Journal of Materials Processing Technology 209(5):2223-30. https://doi.org/10.1016/j.jmatprotec.2008.06.020

[11] Ezugwu EO.(2004) High speed machining of aero-engine alloys Journal of the Brazilian Society of Mechanical Sciences and Engineering 26:1-11. https://doi.org/10.1590/S1678-58782004000100001

[12] Machai C, Iqbal A, Biermann D, Upmeier T, Schumann S.(2013) On the effects of cutting speed and cooling methodologies in grooving operation of various tempers of β-titanium alloy. Journal of Materials Processing Technology 213(7):1027-37. https://doi.org/10.1016/j.jmatprotec.2013.01.021

[13] Rahman Rashid RA, Sun S, Wang G, Dargusch MS.(2011) Machinability of a near beta titanium alloy. Proceedings of the Institution of Mechanical Engineers, Part B: Journal of Engineering Manufacture 225(12):2151-62. https://doi.org/10.1177/2041297511406649

[14] Sun Y, Huang B, Puleo DA, Jawahir IS.(2015) Enhanced Machinability of Ti-5553 Alloy from

Cryogenic Machining: Comparison with MQL and Flood-cooled Machining and Modeling. Procedia CIRP 31:477-82. https://doi.org/10.1016/j.procir.2015.03.099

[15] Bai D, Sun J, Chen W, Wang T.(2017) Wear mechanisms of WC/Co tools when machining high-strength titanium alloy TB6 (Ti-10V-2Fe-3Al). The International Journal of Advanced Manufacturing Technology 90(9):2863-74. https://doi.org/10.1007/s00170-016-9607-z

[16] Ikuta A, Shinozaki K, Masuda H, Yamane Y, Kuroki H, Fukaya Y.(2002) Consideration of the adhesion mechanism of Ti alloys using a cemented carbide tool during the cutting process. Journal of Materials Processing Technology 127(2):251-5. https://doi.org/10.1016/S0924-0136(02)00152-8

[17] Kaynak Y, Gharibi A, Ozkutuk M.(2018) Experimental and numerical study of chip formation in orthogonal cutting of Ti-5553 alloy: the influence of cryogenic, MQL, and high pressure coolant supply. The International Journal of Advanced Manufacturing Technology 94(1):1411-28. https://doi.org/10.1007/s00170-017-0904-y

[18] Tascioglu E, Gharibi A, Kaynak Y.(2019) High speed machining of near-beta titanium Ti-5553 alloy under various cooling and lubrication conditions. The International Journal of Advanced Manufacturing Technology 102(9):4257-71. https://doi.org/10.1007/s00170-019-03291-3

[19] Pimenov DY, Mia M, Gupta MK, et al.(2021) Improvement of machinability of Ti and its alloys using cooling-lubrication techniques: a review and future prospect. Journal of Materials Research and Technology 11:719-53. https://doi.org/10.1016/j.jmrt.2021.01.031

[20] Huang S, Zhao Q, Wu C, et al.(2021) Effects of β-stabilizer elements on microstructure formation and mechanical properties of titanium alloys. Journal of Alloys and Compounds 876:160085. https://doi.org/10.1016/j.jallcom.2021.160085

[21] Sidhu SS, Singh H, Gepreel MA-H.(2021) A review on alloy design, biological response, and strengthening of β-titanium alloys as biomaterials. Materials Science and Engineering: C 121:111661. https://doi.org/10.1016/j.msec.2020.111661

[22] Bania PJ.(1994) Beta titanium alloys and their role in the titanium industry. JOM 46(7):16-9. https://doi.org/10.1007/BF03220742

[23] Yu PJ, Hsu YY, Wang SH, et al.(2020) Comparison of dynamic-aging creep and pre-aged creep in Ti-15-3 beta titanium alloy. Materials Science and Engineering: A 798:140135. https://doi.org/10.1016/j.msea.2020.140135

[24] Klocke F. (2011) Manufacturing Processes 1:Cutting. Springer, Berlin, Heidelberg https://doi.org/10.1007/978-3-642-11979-8

[25] Mouritz AP. (2012) Introduction to Aerospace Materials. Woodhead Publishing, UK https://doi.org/10.1533/9780857095152.202

[26] Vishnu J, Sankar M, Rack HJ, Rao N, Singh AK, Manivasagam G.(2020) Effect of phase transformations during aging on tensile strength and ductility of metastable beta titanium alloy Ti–35Nb–7Zr–5Ta-0.35O for orthopedic applications. Materials Science and Engineering: A 779:139127. https://doi.org/10.1016/j.msea.2020.139127

[27] Wright TW. (2002) The Physics and Mathematics of Adiabatic Shear Bands. Cambridge University Press, UK

[28] Li L.(2004) Study on the Mechanism and Process of High Speed Milling of Titanium Alloys. Dissertation, Nanjing University of Aeronautics and Astronautics [in Chinese]

[29] Krakhmalev PV, Adeva Rodil T, Bergström J.(2007) Influence of microstructure on the abrasive edge wear of WC–Co hardmetals. Wear 263(1):240-5. https://doi.org/10.1016/j.wear.2006.10.019

[30] Bai D, Sun J, Chen W, Du D.(2016) Molecular dynamics simulation of the diffusion behaviour

between Co and Ti and its effect on the wear of WC/Co tools when titanium alloy is machined. Ceramics International 42(15):17754-63. https://doi.org/10.1016/j.ceramint.2016.08.103

[31] Graves A, Norgren S, Wan W, et al.(2021) On the mechanism of crater wear in a high strength metastable β titanium alloy. Wear 484-485:203998. https://doi.org/10.1016/j.wear.2021.203998

[32] Zhang S, Li JF, Deng J X, Li YS.(2008) Investigation on diffusion wear during high-speed machining Ti-6Al-4V alloy with straight tungsten carbide tools. The International Journal of Advanced Manufacturing Technology 44(1):17. https://doi.org/10.1007/s00170-008-1803-z

[33] Odelros S, Kaplan B, Kritikos M, Johansson M, Norgren S.(2017) Experimental and theoretical study of the microscopic crater wear mechanism in titanium machining. Wear 376-377:115-24. https://doi.org/10.1016/j.wear.2017.01.104

[34] Bai DS, Sun JF, Wang K, Chen WY.(2018) Diffusion Behavior and Wear Mechanism of WC/Co Tools when Machining of Titanium Alloy. Solid State Phenomena 279:60-6. https://doi.org/10.4028/www.scientific.net/SSP.279.60

[35] Denkena B, Biermann D.(2014) Cutting edge geometries. CIRP Annals 63(2):631-53. https://doi.org/10.1016/j.cirp.2014.05.009

[36] Bergmann B, Denkena B, Grove T, Picker T.(2019) Chip Formation of Rounded Cutting Edges. International Journal of Precision Engineering and Manufacturing 20(1):37-44. https://doi.org/10.1007/s12541-019-00020-4

[37] Nerz J, Kushner B, Rotolico A.(1992) Microstructural evaluation of tungsten carbide-cobalt coatings. Journal of Thermal Spray Technology 1(2):147-52. https://doi.org/10.1007/BF02659015

[38] Kreimer GS, Vakhovskaya MR.(1965) The effect of carbon content on the mechanical properties of tungsten carbide-cobalt hard alloys. Soviet Powder Metallurgy and Metal Ceramics 4(6):454-9. https://doi.org/10.1007/BF00773965

[39] ZHANG ML, ZHU SG, ZHU SX.(2006) Carbon Content Change and Its Influence on Structure and Properties of Ultraf ine and Nano-cemented Carbide. Materials Reports (08):65-8. [in Chinese]

[40] Bondarenko VP, Pavlotskaya EG.(1997) Hydrogen-containing chemically active gas medium for controlling carbon content of tungsten-base hard alloys. International Journal of Hydrogen Energy 22(2):205-12. https://doi.org/10.1016/S0360-3199(96)00156-5

[41] Hatt O, Larsson H, Giuliani F, Crawforth P, Wynne B, Jackson M.(2016) Predicting Chemical Wear in Machining Titanium Alloys Via a Novel Low Cost Diffusion Couple Method. Procedia CIRP 45:219-22. https://doi.org/10.1016/j.procir.2016.01.196

[42] Hartung PD, Kramer BM, von Turkovich BF.(1982) Tool Wear in Titanium Machining. CIRP Annals 31(1):75-80. https://doi.org/10.1016/S0007-8506(07)63272-7

[43] Hatt O, Crawforth P, Jackson M.(2017) On the mechanism of tool crater wear during titanium alloy machining. Wear 374-375:15-20. https://doi.org/10.1016/j.wear.2016.12.036

[44] Ramirez C, Idhil Ismail A, Gendarme C, et al.(2017) Understanding the diffusion wear mechanisms of WC-10%Co carbide tools during dry machining of titanium alloys. Wear 390-391:61-70. https://doi.org/10.1016/j.wear.2017.07.003